Lipid−Protein Interactions in Lipovitellin[†,‡]

James R. Thompson and Leonard J. Banaszak*

Department of Biochemistry, Molecular Biology, and Biophysics, University of Minnesota, Minneapolis, Minnesota 55455

Received February 13, 2002; Revised Manuscript Received May 22, 2002

ABSTRACT: The refined molecular structure of lipovitellin is described using synchrotron cryocrystallographic data to 1.9 Å resolution. Lipovitellin is the predominant lipoprotein found in the yolk of egg-laying animals and is involved in lipid and metal storage. It is thought to be related in amino acid sequence to segments of apolipoprotein B and the microsomal transfer protein responsible for the assembly of low-density lipoproteins. Lipovitellin contains a heterogeneous mixture of about 16% (w/w) noncovalently bound lipid, mostly phospholipid. Previous X-ray structural studies at ambient temperature described several different protein domains including a large cavity in each subunit of the dimeric protein. The cavity was free of any visible electron density for lipid molecules at room temperature, suggesting that only dynamic interactions exist with the protein. An important result from this crystallographic study at 100 K is the appearance of some bound ordered lipid along the walls of the binding cavity. The precise identification of the lipid type is difficult because of discontinuities in the electron density. Nonetheless, the conformations of 7 phospholipids and 43 segments of hydrocarbon chains greater than 5 atoms in length have been discovered. The conformations of the bound lipid and the interactions between protein and lipid provide insights into the factors governing lipoprotein formation.

Lipovitellin is formed from the proteolytic cleavage of the precursor vitellogenin after the receptor-mediated endocytosis of the lipoprotein by the oocyte. The oocyte receptor is homologous with the low-density lipoprotein (LDL)[1] receptor (*1*). In a manner analogous to LDL, vitellogenin functions to relocate trace minerals and large quantities of hepatic lipid via the bloodstream to the ovaries (*2*). This process is not unlike the function of LDL in higher organisms. In egg-laying species most of the nutritional resources in the oocyte yolk is stored as lipovitellin.

Recently, the conformation of lipovitellin has been of increased interest due to a presumed evolutionary and structural relationship found between the lipoproteins apolipovitellin, microsomal triglyceride transfer protein (MTP), and a segment of apolipoprotein B (apoB). A homologous sequence of more than 670 amino acid residues from the amino-terminal ends of each protein has been described (*3*−*5*). Partial models of MTP and apoB have been published on the basis of the 2.8 Å crystal structure of lipovitellin (*6*, *7*).

The crystal structure of silver lamprey lipovitellin has been developed through a series of experimental steps. The initial polyalanine model was proposed before the vitellogenin cDNA sequence was known (*8*). This 2.8 Å resolution model, obtained using room temperature X-ray data, contained a number of breaks in the continuity of the polypeptide chains. Subsequently, the amino acid sequence and proteolytic cleavage sites of vitellogenin were determined (*9*), and a model with side chains was described (*10*). The second set of coordinates contained 1129 amino acids in 5 polypeptide segments and still had disordered segments. Large cavities for lipid were visible in the structure. Except for a phosphatidylcholine and an unidentified 13-atom hydrocarbon chain, no electron density could be characterized to suggest the nucleation of lipid-binding sites. Nonetheless, the presence of acyl chains within the cavity had been shown by earlier neutron diffraction analyses (*11*).

The sequential and structural labeling of the polypeptide components of lipovitellin is described in detail in Figures 1 and 2 of the report at 2.8 Å resolution (*10*). Proteolysis during oocyte uptake and chain breaks in the electron density map leads to complex domain designations. With regard to the studies described here, the nomenclature is based on the earlier literature of vertebrate vitellogenin (see Figure 1). To summarize briefly, the lipovitellin derived from lamprey oocytes consists of three tightly associated polypeptides of 66.8, 40.8, and 35.2 kDa (SDS−PAGE). The two largest lamprey polypeptides, corresponding to a single sequence in vertebrates, are termed LV1n and LV1c. The 35.2 kDa chain is designated LV2. A fourth, roughly 10 kDa fragment of vitellogenin, named phosvitin, is also found in the lamprey lipovitellin complex. Nearly half of the amino acids comprising phosvitin are serines, and most of these serine residues are phosphorylated (*2*).

All of the roughly 16% (w/w) lipid associated with lipovitellin is noncovalently bound and chemically heterogeneous (*12*, *13*). Depending on the lipid composition, it is estimated that 25−40 molecules of lipid are bound per subunit. Two-thirds are bound phospholipid with the remainder primarily triglycerides, cholesterol, and cholesterol

[†] This research was funded by the NIH (Grant GM13925).

[‡] PDB coordinate file name 1lpv.

* Corresponding author. Tel: 612-626-6597. Fax: 612 624 5121. E-mail: len_b@dcmir.med.umn.edu.

[1] Abbreviations: LDL, low-density lipoprotein; MTP, microsomal triglyceride transfer protein; apoB, apolipoprotein B; ASA, accessible surface area.

10.1021/bi025674w CCC: $22.00
Published on Web 07/04/2002

esters. The complete removal of the lipid results in the inability of the largest polypeptide component to refold. Results using ^{31}P NMR suggest that much of the bound phospholipid exists in some sort of anisotropic phase seemingly either as a monolayer or as a bilayer (*14*). Using this knowledge, molecular dynamics were used to place a hypothetical monolayer of 38 phospholipid molecules within the cavity of a single subunit (*10*) with sufficient volume remaining for the rest of the 4.5% (w/w) of neutral lipid.

Here a successful extension of the X-ray analysis is described. Using low-temperature methods along with rapid synchrotron data collection, a significant increase in the resolution of the X-ray diffraction data set to 1.9 Å was obtained, and visualization of additional bound lipid and protein atoms was possible. The structure provides further details of the interactions between lipovitellin and the bound lipid within.

MATERIALS AND METHODS

Preparation of Lipovitellin Crystals. Lipovitellin from silver lamprey (*Ichthyomyzon unicuspis*) was isolated from the roe of samples from Lake Michigan (under DNR license) using purification protocols described by Meininger et al. (*12*). Buffers, salts, and other reagents were purchased and used without further purification. Crystals were prepared by vapor diffusion in hanging drops at 18 °C. The protein stock was 10 mg/mL lipovitellin with endogenous lipid in 0.25 M sodium citrate at a pH of 6.2. The crystallization conditions include a precipitant range of 0.55−0.61 M sodium citrate at a pH of 6.2 with the additives 1 mM thioglycerol, 1 mM EDTA, and 0.05% sodium azide.

Most crystals of lipovitellin grown were twinned or very mosaic. The single crystal found for data collection was very small, 0.05 mm × 0.05 mm × 0.06 mm. After mounting the crystal in a cryoloop (Hampton Research), preparation for flash cooling was made by a quick dip into a fresh solution of crystallization liquor but with an addition of 25% v/v glycerol. The crystal was then immediately plunged into a Dewar filled with liquid nitrogen and seated within a cryocap (Hampton Research) to allow transfer to the goniometer.

Data Collection and Processing. X-ray diffraction data from lipovitellin were collected using the 19-ID beamline (SBC-CAT), Advanced Photon Source (APS), Argonne National Laboratory, Chicago, IL. A gaseous nitrogen cryostat was used to maintain a temperature of 100 K (Oxford Cryosystems). The tiny size of the crystal resulted in heightened sensitivity to radiation damage. With 1 s oscillation frames of 0.5° width, two scans of 180° were acquired before the falloff in reflection intensity was judged too severe.

The lattice parameters of the crystalline lipovitellin remained essentially unchanged from previous studies, being monoclinic *C*2 with cell dimensions of $a = 190.17$ Å, $b = 84.52$ Å, $c = 89.53$ Å, and $\beta = 100.39°$. The unit cell of the earlier X-ray data at room temperature was $a = 192.7$ Å, $b = 88.4$ Å, $c = 91.5$ Å, and $\beta = 101.3°$. One protein subunit is found within the asymmetric unit. Since lipovitellin and its precursor vitellogenin are homodimers in solution, the crystallographic dyad must relate to the presumed physiological interface present between the subunits.

Table 1: X-ray Crystallography Data Statistics

wavelength (Å)	1.0332
resolution (Å)	30−1.9
unique reflections	82007
OUTLIER rejects (30−5.9 Å)	312
completeness (%)	74.4
Bijvoet redundancy	1.54
$\langle I_{hkl}/\sigma_{hkl}\rangle$	12.2
R_{sym}	0.064

The CCD detector images were indexed, integrated, and scaled using HKL2000 (*15*). Because the high-resolution oscillation scan did not scale well with the second, low-resolution one, the data were not merged. Only the first scan was later used during model refinement. The X-ray data extended to a resolution of 1.9 Å, and the statistics for the single oscillation scan are found in Table 1. The long strands of lipid electron density were found at this stage.

The completeness of the X-ray data and the average signal-to-noise ratio (I_{hkl}/σ_{hkl}) were acceptable. The redundancy of measurements for each integrated reflection is low; consequently, the R_{sym} value is likely to be artificially low. The data quality from the highest amplitude reflections in the range from 12 to 30 Å in part contained some errors discussed in more detail below. Because of higher disorder and heterogeneity, these low-resolution data were later deemed of importance to the structural study of the bound lipid, due to the increased contrast added to the electron density map.

However, before inclusion of the low-resolution data for the refinement of the modeled lipid, the OUTLIER program (*16*) was used to detect rogue observations without relying on the poor redundancy. This program determines expected normalized values from a Wilson distribution of intensities and the model-based structure factor probability distributions. The Wilson distribution is most powerfully used to detect extremely large erroneous measurements; the model-based distributions are best with either very intense or weak outliers. In our case, the model used was the lipovitellin structure determined after rigid body refinement and energy minimization with the 1.9 Å data but without the inclusion of any lipid atoms. The overall *R*-factor was 20.2% (R_{free} 26.3%). OUTLIER assumes an isotropic falloff of diffraction to generate normalized intensity estimates based on a resolution-dependent curve. Because the diffraction pattern from the lipovitellin crystal was not isotropic, first anisotropic *B*-factor scaling (six parameters) was applied to the X-ray data with the program package CNS (*17*). This reduced the risk of rejecting legitimate observations. Out of the 3289 intensity measurements from 5.9 to 30 Å, 312 were flagged suspect and thereafter ignored.

Model Refinement. The model refinement began with the lipovitellin structure determined at 2.8 Å resolution minus any heteroatoms (*10*). The starting *B*-factors were initialized to 20.0 Å^2. A random "free" data set of 983 reflections was marked for cross-validation purposes across a resolution range of 30−1.9 Å. This entire range of X-ray data was used for model refinement and electron density map calculations.

The X-ray refinement was completed with CNS, version 1.0 (*17*). In addition to cross-validation, an overall anisotropic temperature factor correction, a bulk solvent correction, and maximum likelihood targets were used in CNS. Two

programs, O (*18*) and MAID (*19*), proved helpful during periods of model rebuilding and for real-space refinement into electron density maps. At first, the method involved rigid body, simulated annealing and then positional refinement (Powell) using the standard Engh and Huber (*20*) force field incorporated into CNS. Repetitive cycles of model building and energy minimization followed. Canonical parameters were monitored by CNS, WHATCHECK (*21*), and PROCHECK (*22*). Extensive use was made of the most recent rotamer database of amino acids (*23*).

The first water molecules were added when the *R*-factor reached 24.9% (R_{free} 28.6%), but only when spherical $2F_o - F_c$ and $F_o - F_c$ electron density was observed at 1σ and 3σ, respectively, and a heteroatom existed 2.5−3.6 Å from this density. Using these rules, 593 waters were initially added to the model, refined, and then rechecked. The addition of these water molecules to the model improved the *R*-factor to 22.1% (R_{free} 26.8%). Construction of the rest of the bound solvent structure was automated with algorithms found in the programs WARP (*24*) and CNS. The program DDQ (*25*) was used to complement the procedures in CNS to validate the solvent positions. DDQ differentiates putative solvent peaks in a $F_o - F_c$ electron density map, calculated with the waters intentionally removed, from shift peaks caused by errors in atomic placement or temperature factor. In later iterations of refinement, solvent molecules were removed if their temperature factors surpassed 100 Å^2 or their location moved by more than 2.0 Å.

After further progress (*R*-factor 20.2%, R_{free} 26.3%), the lipovitellin model was used to search for structure factor outliers in the low-resolution range. A significant improvement in electron density maps was observed after 312 reflections were rejected. Importantly, increased contrast and fewer discontinuities were found in regions of disordered polypeptide as well as that encompassing the binding cavity. Another advance resulted from small changes made to the Engh and Huber geometric parameters to better reflect new empirical data from very high resolution structures refined both with and without geometric constraints (*26*−*29*).

Lipid molecules were modeled at this point, but only if an appropriate fit could be made with a hydrocarbon chain of five or more carbons in length. In the end, some electron density above the 1σ contour level remained that was not explainable by a bound water structure and, in our view, is not complete enough to model with hydrocarbon chains. The original coordinates for phospholipid molecules were obtained from the Cambridge Structural Database using QUEST (*30*). During the ligand modeling and refinement process, the *B*-factors of individual atoms were refined. Moreover, preliminary stereochemical restraints applied to the lipid molecules were relaxed in the last stages of refinement to values (*31*) which allowed a better fit to the corresponding electron density. Despite much effort, unambiguous chemical identification of these "lipid-like" features of the electron density proved impossible. For one stretch of hydrocarbon modeled, there remains the possibility that the electron density is actually highly disordered polypeptide rather than lipid (discussed below).

RESULTS AND DISCUSSION

The most significant result of this study is the new information about the presence and organization of bound lipid molecules within lipovitellin. Most of the visible lipid sites interact with a portion of the interior cavity surface, although only portions of this first layer of bound lipid can be defined. The binding interface of a fifth of the lipid molecules observed results primarily through lipid−lipid interactions (see below), analogous to a second layer of lipid fixed to the first shell. The observation of partial nucleating shells of methylene chains seems analogous to bound solvent structures commonly found at the surfaces of proteins. To differentiate from the relatively larger, unobserved fraction of lipid present in the lipovitellin cavity, the immobilized portion will be referred to as boundary lipid.

Table 2: Average *B*-Factor Comparison[a]

	1.9 Å cryotemp		2.8 Å room temp	
	no. of atoms	av *B*	no. of atoms	av *B*
protein main chain	4595	41.8	4521	62.3
protein side chain	4543	47.9	4297	66.3
protein, all atoms	9138	44.8	8818	64.3
water molecules	1122	66.3	59	43.5
phospholipids	284	73.5	40	38.8
	(57	49.8)		
hydrocarbon chains	373	78.3	13	44.2
	(16	47.9)		
all atoms	10917	48.9	8930	64.0

[a] The values within parentheses are for the phospholipid and the hydrocarbon chain in common between both structures. Atoms with zero occupancy are not included.

Quality of Model and Map. Shown in Table 2 is a comparison between the cryocrystallographic model of lipovitellin and that obtained at room temperature. The number of atoms and their average temperature factors are listed for the protein and ligands. A secondary result of this study is a significant improvement realized for the X-ray coordinates of the lipovitellin model. Note the data in Table 2 showing a general decrease in thermal disorder for protein atoms and an increase in observable lipid atoms compared to the earlier model. The phosphorylated polypeptide segments described in the introduction and known to be present in the crystals still remain disordered (*10*). The thermal ordering of protein atoms likely imparts similar order to lipid molecules in the nearby vicinity. The fact that the average *B*-factors of ligands are higher in the 1.9 Å structure is a function of their increase in number in the coordinate list. An overall decrease in *B*-factors for the identical ligand atoms is found as expected but is not shown.

The results from refinement and the model statistics are contained in Table 3. The differences between the *R*-factor and R_{free} are centered within the empirically observed range for the resolution of the X-ray data (*32*). Segments of the final electron density map will be presented in a later section discussing the presence of the lipid shell. The final difference map was reasonably flat, with a standard deviation of 0.55 e Å^{-3} before normalization. A notable negative peak ($>4\sigma$) is found in the center of the lipid-binding cavity far from any modeled atoms. This peak may be due to the assumption of an average electron density equaling that of water that was applied and implicit in the bulk solvent correction. No attempt was made to define the average electron density of the lipid-containing cavity independent of the solvent regions surrounding the molecule.

Eleven hundred and twenty-nine residues were modeled, the same amount as in the original study at ambient

Table 3: Model Refinement Statistics

PDB ID code	1LSH
resolution	30−1.9 Å
R_{factor}	0.193
R_{free}	0.255
reflections (working)	80712
reflections (free set)	983
coordinate error[a] (5.0−1.9 Å)	0.28 Å
coordinate error[b] (5.0−1.9 Å)	0.28 Å
av *B*-factor	48.9
min *B*-factor	8.5
max *B*-factor	100.0
B rmsd bonded main chain atoms	4.76
B rmsd bonded side chain atoms	7.04
B rmsd angle main chain atoms	6.02
B rmsd angle side chain atoms	9.00
rms bonds	0.019 Å
rms bond angle	2.50°
rms dihedral	25.7°
rms improper	2.45°

[a] Cross-validated Luzzati. [b] Cross-validated sigmaa. Luzzati and sigmaa plots were calculated with 5−1.9 Å data.

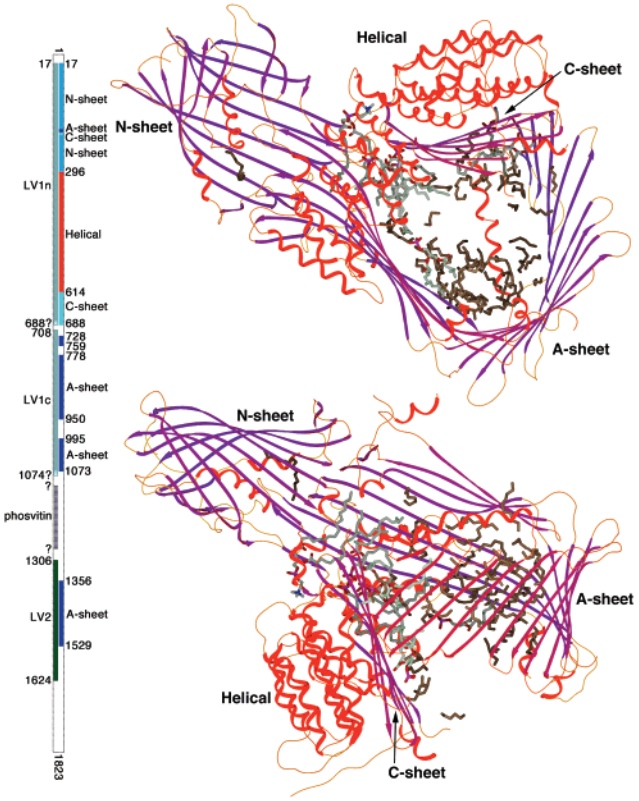

FIGURE 1: Overall structure of the lipovitellin at 100 K. Two views are shown of the ribbon structure of the present crystallographic model of lamprey lipovitellin with bound lipid. The nomenclature used to describe the original structural study is maintained (*10*). A color gradient from blue (background) to maroon (foreground) is used for the ribbons representing β-strands to provide depth. All α-helices are in red. The thin, yellow-orange linking segments are loops and meandering coil. The upper image was composed to best show the interior of the lipid-binding cavity at the bottom right. The lower picture was oriented to provide some perspective but also a clearer idea of the cavity shape and contents. The amino terminus of the protein is to the top left in both views beginning with the N-sheet domain and with the helical domain following. The C-sheet lines the inner side of the helical domain. Finally, an extensive A-sheet completes the polypeptide structure. The binding cavity is mainly surrounded by the inward-pointing side chains of the C- and A-sheets. The bars at the left indicate how the single polypeptide chain of vitellogenin is proteolytically cleaved while being taken up by the ovaries. The components of this sequence visible in the electron density map are denoted by the bars to the right. In the case of lamprey, multiple segments are formed. Only LV1n, LV1c, and LV2 are visible in the model. LV1n contains the N-sheet, the helical domain, and regions of the two β-sheet structures surrounding the lipid cavity, the A- and C-sheets. The LV1c and LV2 proteolytic segments form the remainder of the C-sheet that is observed. The brown-colored model segments represent the positions of hydrocarbon chains. Finally, portions of phospholipid molecules are visible with gray-green carbon atoms.

temperature. Sixty-nine amino acids were included with two discrete conformations; 50 of these are within LV1n. There is a single residue sequence deletion at Gln838 compared to the lipovitellin cDNA and structure at 2.8 Å. The electron density for the loop conformation in this locale does not appear to support the presence of Gln838. Nonetheless, the residue numbering scheme continues to match amino acid positions found in the precursor vitellogenin polypeptide but with a gap at position 838. Side chain atoms of residues 501, 524, 759, and 1480 could not be located, and their occupancies were set to zero. Not including these missing side chains, the model consisted of 9138 protein atoms and 657 atoms believed to be parts of lipid molecules. Of the latter, 284 atoms are interpreted as phospholipid (portions of 7 molecules), 373 atoms belonging to 43 hydrocarbon chains each longer than 5 atoms in length. In addition, there were 1122 water atoms forming the bound solvent structure.

The stereochemical quality of the lipovitellin model is very good, with over 89% of the amino acid residues in the most favorable regions of the Ramachandran plot (determined by PROCHECK; data not shown). Another 9.4% are in the additionally allowed regions. There are two side chain outliers, Lys1357 and Ser1386, which though supported by electron density have very high *B*-factors. The two residues occupy a γ-turn region of the Ramachandran plot near +70°, −60° missed by PROCHECK. This combination of torsional angles has been recently recognized to be lightly populated (*33*). The model accuracy is reflected by overall coordinate uncertainties of 0.31 Å [Luzzati plot (*34*)] or 0.27 Å [by sigmaa plot (*35*)]. PROCHECK classified the model as being of excellent quality and consistent with other structures of similar resolution. The coordinates of lipovitellin have been deposited in the Protein Data Bank, with the identification code 1LSH.

Lipovitellin Model. While the principal focus of this report is to describe the electron density that is observable for the bound lipid within the lipoprotein cavity, the surrounding protein is also important since it is the framework for the lipid. Ribbon diagrams of lipovitellin complete with ordered lipid are shown in Figure 1. In the interest of brevity and clarity, Figure 1 ignores the fact that lipovitellin is a dimer with 2-fold symmetry. All descriptions of the conformation of protein or lipid apply to both subunits.

Shown in the leftmost portion of the bar in Figure 1, LV1n is the polypeptide segment at the amino terminus. It forms two domains and portions of two more: the N-sheet, the helical segment, one β-strand of the A-sheet, and all but two β-strands of the C-sheet. The amino acid sequence attached to LV1n includes pyroglutamate 17 to at least Tyr688. In lamprey lipovitellin, the cleavage site between LV1n and LV1c is thought to be somewhere between residues 700 and 708. The two final β-strands of the C-sheet comprise Asp728

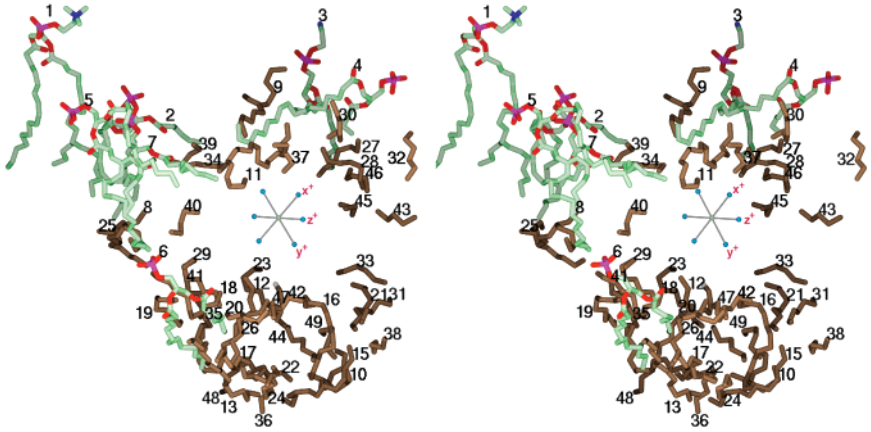

FIGURE 2: Bound phospholipid molecules and hydrocarbon chains exposed. The cross-eye stereo diagram presents the relative orientation and conformation of the boundary lipid found within the 100 K lipovitellin structure. Shown are 7 phospholipid molecules in green and 43 hydrocarbon chains in brown. They range from 5 methylene carbons on up to 57 atoms. The orientation in Figure 2 corresponds to the top view in Figure 1. The marker in the center of the lipid-binding cavity marks the direction of the crystallographic axes. It was placed in the cavity core where more disordered lipid molecules reside to help view the varying directional nature of the methylene chains.

to Met759 of LV1c. The A-sheet domain is a β-sheet with four peripheral helices formed by both LV1c and LV2. Gln778−Thr950 and Gln995−Gly1073 from LV1c form the portion of the A-sheet directly opposite from the C-sheet and a bulge that changes the direction of the remainder of this β-sheet to enclose the lipid cavity. Defining the four separate domains was an arbitrary decision based more on secondary structure rather than any attempt to define independent folding units. Also indicated by the bar graph in Figure 1 are stretches of unobserved polypeptide that according to chemical analyses are nonetheless present in the crystals. Of note are a missing link between the C- and A-sheets, phosvitin, and residues probably near a cavity opening.

The N-sheet domain mainly consists of 11 β-strands wrapped around an uncharged helix of 14 residues, although another β-strand and 3 more small helices are included. In Figure 1, this domain is found at the upper left in both images. There are two disulfide bonds within this region; one is conserved in the homologous proteins MTP and apoB. A drawn out loop containing two β-strands helps to link the N-sheet to both the C- and A-sheets. In addition, a depression in the N-sheet globular domain accepts the loops of several β-strands from the C- and A-sheets forming multiple interactions. Past comments have suggested the region has the appearance of and may function as a flexible "ball-and-socket" joint accommodating the lipid as the lipoprotein assembles (*10*). In addition to this discussion, a tabulation and enumeration of domain−domain interactions is found in Anderson et al. (*10*).

An extensive helical domain follows with a conformation best described as a superhelical right-handed, coiled coil with a two-helix repeating unit. The band of α-helices is located at the midpoint of the lipovitellin molecule in Figure 1. There are 18 helices in this domain, and this superhelical conformation has now been described in other crystal structures. The two-helix repeating pattern results in an appearance of two layers of helical structure that form an arch. This arch then forms a clasp around the β-sheet structures. The helical domain has a substantial buried hydrophobic volume.

The lipid cavity is covered with residues forming the C-sheet and the A-sheets. There are very few interactions between the two β-sheets. The seven β-strands of the C-sheet line the carboxy-terminal half (thus "C" sheet) of the helical domain. Extensive interactions also occur between the A-sheet and the amino-terminal end (thus "A" sheet) of the helical domain. The A-sheet is larger, containing 24 β-strands. The C-sheet is best found in the bottom picture of Figure 1 to the right of the helical domain.

The Boundary Lipid. Except for one molecule buried within a hydrophobic cavity in the N-sheet, all other visible lipid molecules were found along the walls of the interior-binding cavity. Shown in the stereo image of Figure 2 is the shell-like nature of the boundary lipid. The hydrocarbon chain in a second binding cavity (lipid 14 in the coordinate list) is not in Figure 2. In all, 43 hydrocarbon chains (brown) and 7 phospholipids (gray-green) are present. The greatest number of phospholipid molecules are found where the cavity narrows and interactions with protein atoms increase at the juncture of the N-terminal domain and both β-sheets, the region referred to earlier as a ball and socket. Such a pivot point may allow movement of the C-terminal β-sheet and possibly provide a mechanism for lipid loading and removal. In this area, some protein interactions with phospholipid headgroups are found. Enclosing the polar end of lipid 1 are regions with the lowest atomic *B*-factors of lipovitellin.

The molecules in Figure 2 also convey the fact that most of the observed hydrocarbon chains are generally shorter than expected for physiological phospholipid molecules. Recall that a minimum acceptable length was arbitrarily set at five carbon atoms and the actual chain length is not identifiable. There are a few likely explanations for this difficulty, all of which may apply. Any visible portion must be ordered throughout the crystalline lattice. However, the acyl chains from more than one lipid molecule may also fill the same crystallographic location. Moreover, any given binding site may be occupied by a chemically diverse assortment of atoms, due to (a) differences in the lipid type, (b) differences in the extent of the same carbon chain, or (c) differences in the frequency and location of unsaturated bonds.

In the central region of the lipid domain (Figure 2) is shown a marker denoting the direction of the crystallographic axes. The marker should serve as a symbol to reference the directional packing of the visible hydrocarbon atoms. It also

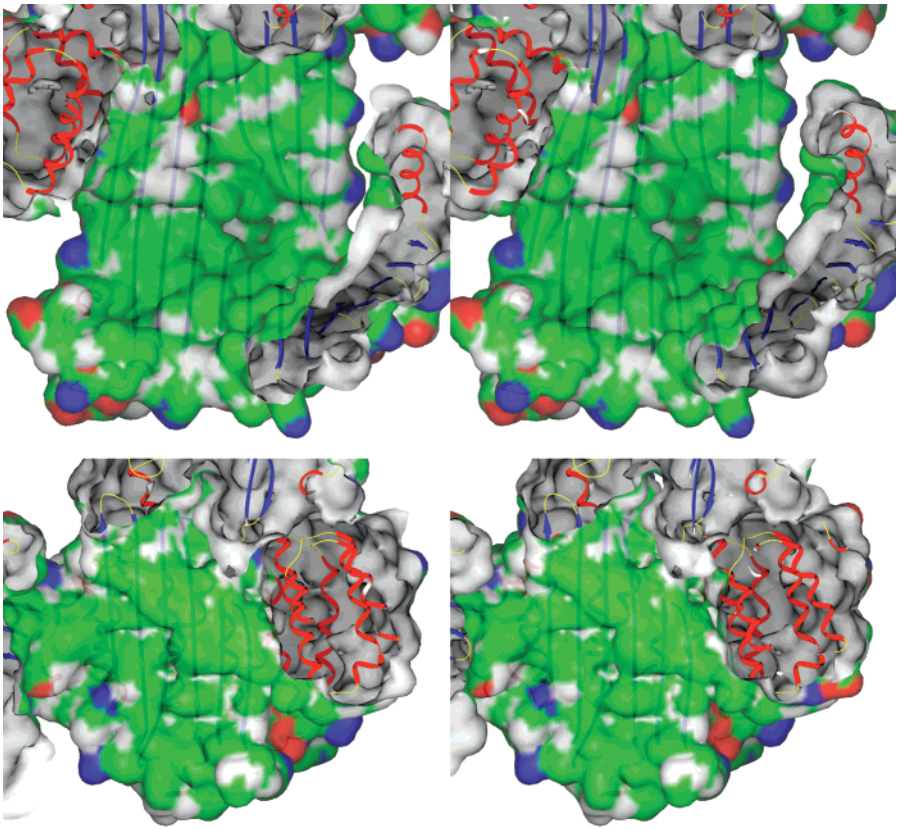

FIGURE 3: Molecular surfaces of the lipid-binding cavity. The cavity in which the lipid binds is mainly hydrophobic in character. The top cross-eye stereo diagram shows most of the solvent-accessible surface of the A-sheet domain that faces the lipid-binding cavity. The lower picture provides a similar view of the C-sheet, opposite from the A-sheet. The surface created by nonpolar atoms is colored green. The blue and red colored surfaces are formed from the few basic and acidic residues, respectively. A ribbon cartoon representing the lipovitellin main chain is provided for orientation and perspective.

marks part of the volume that must contain the disordered lipid molecules, those that are not visible in the electron density map.

Earlier NMR studies had suggested the presence of lipid in an anisotropic environment corresponding to phospholipid in a mono- or bilayer-like phase (*14*). Although the accommodated boundary lipid initially appears to have an almost random orientation, this is not entirely the case. For example, the tails associated with lipids 6, 13, 17, 18, 19, 24, 29, 36, and 47 appear to bind in an approximately parallel mode (see Figures 2 and 4B). Other small domains of bilayer-like chains are also visible. With the major portion of the bound lipid not visible, the overall lipid organization is difficult to define. The presence of a mono- or bilayer-like organization in the disordered segment remains a reasonable hypothesis.

Lipovitellin's Cavities. Using the algorithm implemented in the program CAST (*36*), it is possible to define 162 cavities or pockets in the lipovitellin structure. For the majority their significance, if any, is unknown. Some may be due to protein segments not visible in the electron density map. Three of the cavities are relatively large, and their surface areas and volumes are tabulated in Table 4. The principal lipid-containing volume readily visible in Figure 1 measures about 60000 Å^3. A second small volume occupied by lipid 14 within the N-sheet domain is 643 Å^3. Interestingly, another cavity volume of 722 Å^3 is completely enclosed and resides between the interface of the helical and C-sheet domains. This third cavity is filled with bound solvent.

Table 4: Volume and Surface Area of Three Cavities[a]

	main	helical	N-sheet
mouth openings			
molecular	7	0	1
accessible	3	0	1
cavity volume (Å^3)			
molecular	59584	722	643
accessible	42770	64	137
surface area (Å^2)			
accessible (ASA)	11158	262	245
molecular	13282	745	505
ASA (%)			
nonpolar	77	82	83
polar	15	11	9
positive charge	6	4	6
negative charge	1	5	2
sulfur	1	0	0

[a] The cavity volumes and areas were found with CAST (*36*). The three molecular surfaces are essentially formed by use of the atomic van der Waals radii of surrounding residues, while the accessible surfaces trace the center of a 1.4 Å probe molecule as it rolls over the molecular surface. Only the three openings into the main cavity found in the accessible surface appear to be relevant with regard to the lipid-binding function of lipovitellin. The percentage compositions regarding the nature of the solvent-accessible surfaces were determined using the cavity extents output from CAST.

Listed in Table 4 is the percentage of the accessible surface area (ASA) for the three largest cavities in terms of the nonpolar, polar, charged, or sulfur-containing (Met, Cys) nature of its underlining atoms. The distribution of the nonpolar, polar, and charged nature of the surface for the principal cavity is shown in Figure 3. The top image is the

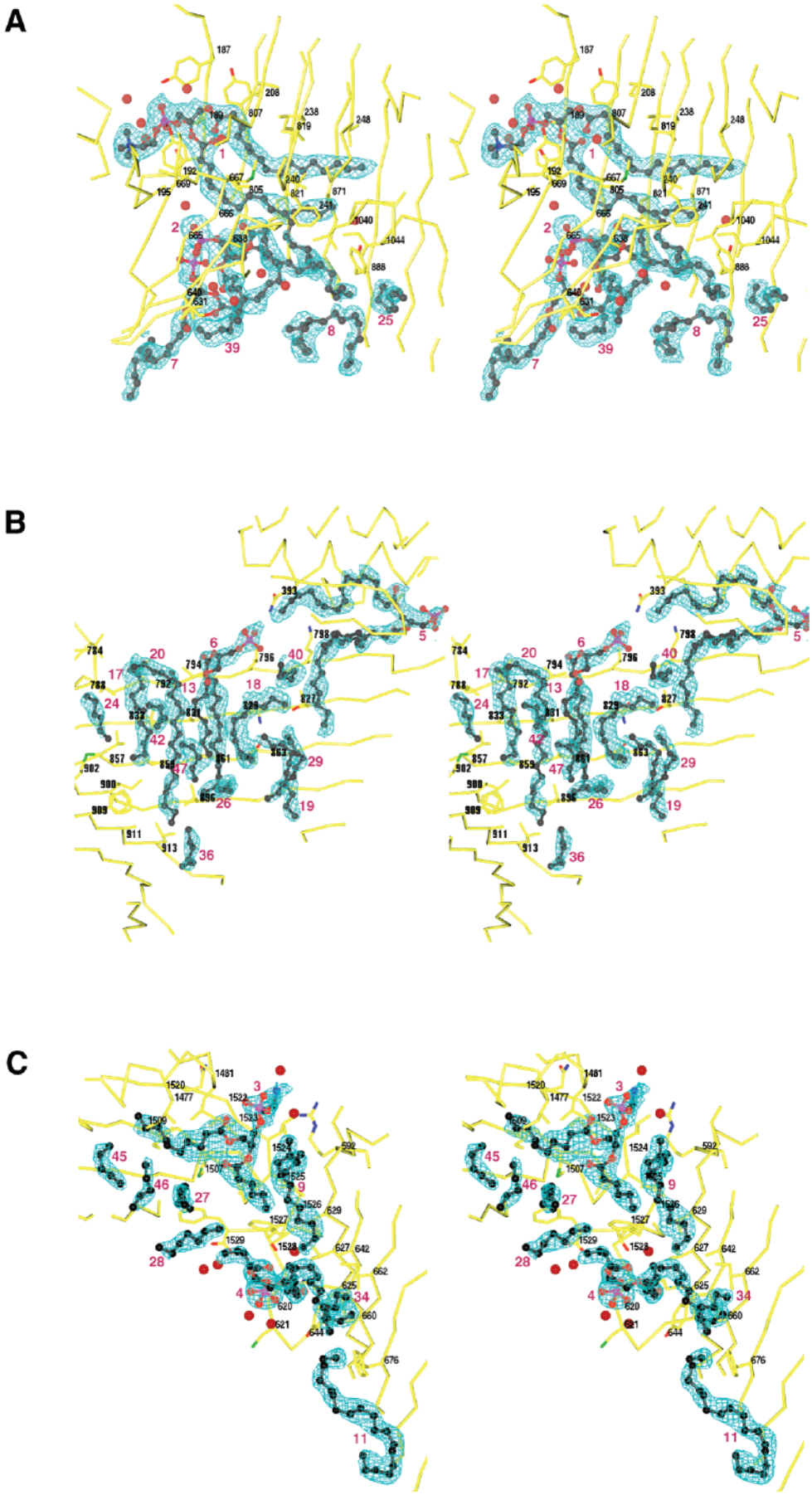
A
B
C

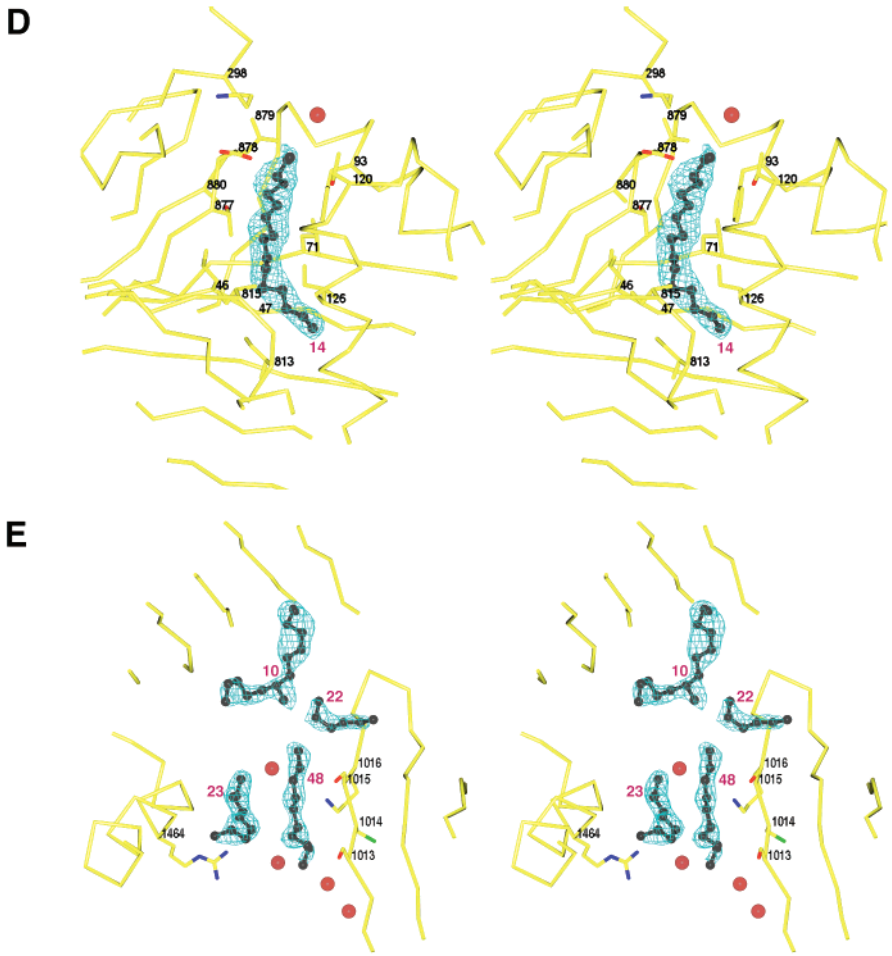

FIGURE 4: Interactions and electron density for lipid molecules. Cross-eye stereo diagrams are shown with portions of the bound lipid component, their electron density in a $2F_o - F_c$ omit map, and the nearby lipovitellin and water structure. These omit maps, colored a gray-blue, are contoured at the 1.0σ level. Due to the number of modeled hydrocarbon chains and their locations about the cavity walls, all of the lipid molecules will not be shown. (A) Three of the phospholipid molecules are clearly visible. The map density for the upper molecule (lipid 1) suggests the presence of a choline headgroup, and diacylphosphatidylcholine was modeled. One of the hydrocarbon chains shows discrete disorder. The headgroups of the lower phospholipids, numbers 2 and 7, are disordered beyond the phosphate. (B) Portions of two more phospholipid molecules are shown, lipids 5 and 6. The headgroups of both are unobserved past the phosphate atoms. The polar headgroup of number 6 extends out through the largest opening in lipovitellin's binding cavity into the external solvent. There is an appearance of a monolayer or bilayer organization to the lipid. (C) Two phospholipid molecules and unknown lipid at the opposite end of the cavity opening depicted in (B). Lipid 3 is modeled as phosphatidylethanoamine (top); it is the only lipid found interacting with the other lipovitellin molecule in the dimer present in solution. Notice the largely parallel orientation of the hydrocarbon chains, maximizing lipid−lipid van der Waals contacts. The lipids also are roughly perpendicular to the alignment of the main chain forming the C-sheet (right). (D) This figure illustrates the sole lipid molecule found bound to a pocket within the N-sheet. The nature of lipid 14 is unknown, and the binding pocket has no connection to the main lipid-binding cavity. As within the main cavity, the predominant interactions are hydrophobic. (E) A region of the smaller opening into the cavity is shown where many hydrocarbon chains were modeled into electron density. The observation that one hydrocarbon chain parallels the edge of the most exposed β-sheet (center top) causes some concern in regard to the assignment of this feature as lipid. It is possible that the electron density shown in the gap is due to atoms belonging to a disordered polypeptide segment, though little information indicates which lipovitellin residues might occupy the site.

surface over the A-sheet while the lower is that belonging to the C-sheet. The surface is in green over side chains that are hydrophobic in nature; charged basic residues are in blue and acidic amino acids are in red. Side chains that line the cavity walls are mainly hydrophobic.

The main lipid-binding cavity is shaped much like a funnel with two major openings to the external solvent. A third large opening, seen in the monomer structure, is not present in the dimer normally existing in solution. In contrast to the inner surface, a few ionizable residues exist around the rim of the largest opening. There are four additional but very diminutive openings to the cavity's molecular surface of probably lesser significance. The boundary lipid is primarily found adjacent to the nonpolar portions of the accessible surface shown in Figure 3.

Lipid Binding Mediated Chiefly through van der Waals Interactions. Electron density describing the boundary lipid along with the immediate protein surroundings is shown in stereo in Figure 4. The locations of any nearby solvent molecules are also indicated, but not all 50 lipid fragments are presented. The omit maps are contoured at the 1.0σ level, and all density is shown within 2.0 Å of any lipid atom. Note that we have given each lipid molecule a number from 1 to 50 and the same number is present in the PDB coordinate file.

Figure 4A provides the view of the lipids and surroundings at the ball and socket of lipovitellin. The image was limited to the atoms neighboring lipids 1 and 2. The binding site for number 1 is formed in part by a polypeptide loop present in the N-sheet, residues 185−206. A smaller portion of lipid

Table 5: Molecular Interactions for the Boundary Lipid in Crystalline Lipovitellin[a]

Lipid	Lipovitellin residues	Other Lipids	Waters
1	*Y187 T189 T192 A193 A195 E196 R197 N207 L208 L238 V240 F241 V248 A444 N445* **G666** *M667 Y669 V805 Y807 L819* **N820** *L821* **V823** *A869 A871 I872 M873 M884 T886 Y888 L1041 I1044*	*2 7 8*	**23** *20*
2	**A195** *V240 F241 T631 N633 T636 A638 G639 V640 G664 Q665 G666 M667 Y669* **A670** *S671 I673 L821 Y888* **M927** *L1040* **K1043** *I1044 Y1048*	*1 7 8 9 25 39*	**11** *10*
3	*R592 V629* **D630** *N1038† A1474 I1477* **A1478** *L1481 M1483 M1507 I1509 V1511 Y1518 Q1520 G1522 I1523 L1524 L1525 P1526 F1527*	*4 9 27 28 45 46*	**3** *2*
4	*G620 C621 K625 V627 V629 A642 Y644 R646 A660* **K661** *I662 V674 F676 F1527 T1528 F1529*	*3 9 11 27 28 34*	**6** *6*
5	*G191 Y194* **P366** *T392 Q393 A396 S397 S400 N401* **I426** *T430 G434* **R441** *V745 H746* **Q748** *V750 V751 K798 Y800 V801 V802 S803* **E804** *T827 M865 Q867*	*7 8 11 18 19 29 40*	**17** *17*
6	*Q393 V794 L796 K798 N829 A831 A861* **T862** *T863 L894 V896*	**12** *13 17 18 20 26 40 42 47*	**3** *3*
7	**A396** *S671 I673 V674 F676 V743 V745 H746 V750 V751 V802 S803 V805 L821 V823 Q867 A869*	*1 2 5 8 11 34 39 40*	**6** *5*
8	*V823 M865 Q867 A869 Y888 T890 V923 S925 F1026 Y1048* **S1050**	*1 2 5 7 25 29 35 39 41*	**5** *5*
9	*R592 S593* **S594** *V629 D630 T631 F632 V640 A642 I662* **L1524** *P1526*	*2 3 4 39*	**7** *6*
10	**K1016** *L1376 T1378 I1394 A1396 W1405 L1407 I1423 W1425* **P1459** *L1462*	*15 21 22 31 44 48 49*	**7** *7*
11	*I426 Y644 V658* **A659** *A660 F676 L678 G741* **Y742** *V743 V751 A753*	*4 5 7 30 37*	**2** *2*
12	*L894 F916 V922 V923 V1024 V1052 V1054*	*6 16* **18** *19 22 26 29 35 36 50*	**3** *3*
13	*M792 V794 A831 L833 L857 V859 A861 V896 I900 F909 A911 L913 V1066*	*6 17 20 26 36*	**1** *1*
14	*A30 L46 S47 G48 M50 L71 L86* **Y90** *F93* **Q96** *T120* **T122** *I126 K298 I813 I815 T877 D878 L879 A880*		**8** *8*
15	**K1016** *S1017 A1019 L1020* **V1066** *I1362 L1364 L1376 T1378* **L1380** *I1394*	*10 16 22 31 36 38 44*	**3** *3*
16	*V1066 L1068 I1362 L1364*	*12 15 26 31 36 38 44 50*	**0** *0*
17	*V784 L788 M792 L833 L857* **V859** *I900 M902 F909*	*6 13 20 24 42*	**0** *0*
18	*L796* **K798** *T827 N829 T863 M865*	*5 6* **12** *19 26 29 40* **47**	**0** *0*
19	*T827 N829 T863* **S864** *M865 A892* **G893** *L894 V922 V923* **V1052**	*5 12 18 29* **35**	**1** *1*
20		*6 13 17 24 42*	**2** *1*
21	**L1407** *I1423 W1425 A1434 I1453* **W1455** *L1458 L1462 K1466* **L1470**	*10 31 33 49*	**0** *0*
22	*S1015 K1016 S1017* **L1020** *V1024*	*10 12 15 44 48*	**4** *4*
23	*S1461 L1462 A1465 A1468 L1469*	*48* **49**	**0** *0*
24	**I781** *V784 L788* **L847** *L850* **L851** *I855 L857* **I900** *M902*	*17 20*	**1** *0*
25	*Y888 M927 R1009 L1030* **N1032** *K1043 I1044 Y1048*	*2 8*	**8** *6*
26	*L894 V896 L913*	*6 12 13 16 18 36 47*	**1** *1*
27	*V1497 L1499 M1507 I1509* **F1527** *F1529*	*3 4 28 46*	**0** *0*
28	*V1451 L1499 F1527*	*3 4 27 43 46*	**0** *0*
29	*M865*	*5* **8** *12 18 19*	**0** *0*
30	*Y644 L654 P655 V658 L678 A680*	*11*	**2** *1*
31	*I1394 L1407 A1409 A1421 I1423 L1436*	*10 15 16 21 33* **44** *49*	**1** *0*
32	*P653 L654 L687*		**2** *2*
33	*I1423 A1434 L1436 I1453* **L1462**	*21 31*	**0** *0*
34	*I662 I673 V674 F676*	*4 7 39*	**2** *1*
35	*V923 S1013 S1015 V1024 F1026 V1052*	*8 12 19 41*	**1** *0*
36	*L913 L1020 T1064 V1066 L1364*	*12 13 15 16 26* **47**	**3** *3*
37	*L678 A739* **S740** *G741 A753 L755*	*11*	**0** *0*
38	*L1068 L1070 V1360 I1362 L1380 Y1382* **I1394**	*15 16*	**0** *0*
39	*V640 I662 I673*	*2 7 8 9 34*	**2** *2*
40	*K798*	*5 6 7 18*	**0** *0*
41	*S1013 F1026 V1052*	*8 35*	**4** *3*
42		*6 17 20 47*	**0** *0*
43	*F1411 A1419 L1436 A1438 V1451*	*28 46*	**1** *1*
44		*10 15 16 22 49 50*	**0** *0*
45	*I1453* **L1469** *L1470 A1474 I1477 V1495 V1497 V1511 L1513*	*3 46*	**0** *0*
46	*V1451 I1453* **L1481** *V1497 L1499* **I1509** *V1511*	*3 27 28 43 45*	**0** *0*
47		*6* **18** *26* **36** *42*	**0** *0*
48	*S1013 C1014 S1015 K1016 R1464*	*10 22 23*	**5** *5*
49	*L1407 I1423* **W1425** *L1462*	*10 21* **23** *31 44*	**0** *0*
50		*12 16 44*	**0** *0*

[a] Interactions in italics are due to atomic contacts. The bold text indicates interactions that are due solely to the loss of more than 1 Å^2 of accessible solvent area (ASA). The lipid numbers correspond to the residue numbers found in the PDB file. The number of interfacial solvent molecules that lost ASA or are in atomic contact are given in the rightmost two columns. †: lipid 3 forms the only lipid interaction with an amino acid from a symmetry-related lipovitellin monomer.

1 was found in the 2.8 Å lipovitellin structure. The map density and surrounding protein interactions for number 1 suggest the presence of a choline headgroup. The phosphate atoms of the headgroup form hydrogen bonds with residues Y187, T189, and T192 (top, background). In addition, one of the hydrocarbon chains shows discrete disorder. Of special note are the extensive van der Waals interactions formed with lipid 1. This represents the burial of nonpolar amino acids from the N-, C- and A-sheets. Table 5 contains a list of the lipid−protein, lipid−lipid, and lipid−solvent interfaces defined by atomic contacts and the loss of accessible surface.

The headgroups of two other nearby phospholipids (numbers 2 and 7 in Figure 4A) are disordered beyond the phosphate, and the phosphate atoms have very high *B*-factors. Each of these molecules buries about half as much of the protein ASA compared to lipid 1. Expanding somewhat outward from the confines of Figure 4A, the phosphodiester atoms of lipids 1, 2, 5, and 7 are clustered. Many bound waters exist within this peptide-enclosed volume. However,

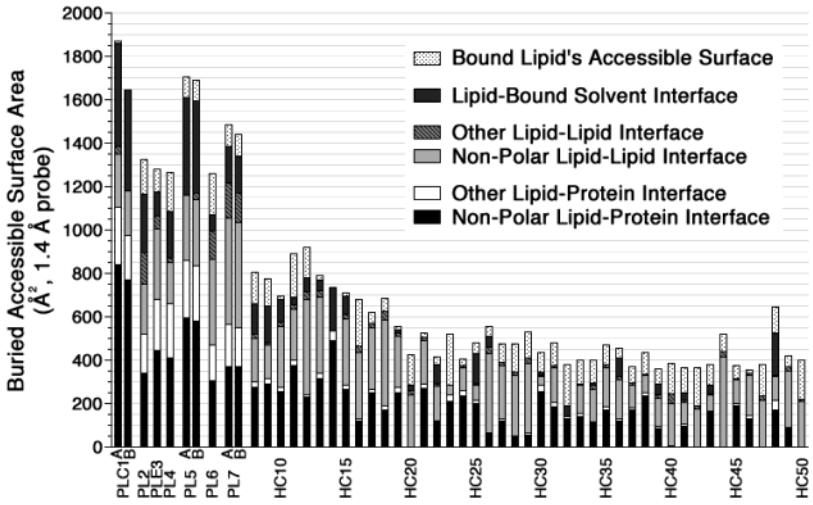

FIGURE 5: Lipid−protein and lipid−lipid interactions in lipovitellin. Each of the 50 segments of lipid molecules is analyzed in terms of the buried accessible surface area (ASA). Each buried ASA value results from the calculation of (molecule A's ASA + molecule B's ASA) − (the molecular complex of AB's ASA). The reader is reminded that in many cases only fragments of the bound lipid are observed. The areas for five different buried interfaces are defined by the shading of each bar, which sum to the total buried ASA for each lipid (see the key contained in the graph). Finally, the ASA of each bound lipid is also indicated at the top of the bars. Note that it is presumed that the interior volume of the main binding cavity is filled with disordered lipid. For lipids 1, 5, and 7, multiple conformations were computed separately.

some may represent the disordered atoms of the unobserved portions of the polar headgroups. The phosphodiesters of lipids 2 and 7 are close enough that they interact. Much like the presence of two negatively charged side chains in a globular protein, this is possible on the basis of the location of negative charge. Examination of the protein surrounding the phosphodiester center of lipid 5 reveals hydrogen bonds to Y194 and R441 (not shown). Interestingly, one acyl chain for both lipids 5 and 7 is modeled with two conformations.

Figure 4B contains a representation of a total of 14 of the reported lipid coordinates, including two more partial headgroups (numbers 5 and 6). The phosphate moiety of number 6 has high *B*-factors and appears to be closest to a neutral polar residue, Q393, and the basic side chain of K798. Beyond the phosphodiester, the polar headgroup atoms belonging to both molecules must be completely disordered. The disorder of these atoms for number 6 may relate to their extension out into the external solvent from what is the largest opening in the binding cavity.

Figure 4B also contains data that suggest the lipid domain may partially pack together with the hydrocarbon chains in a monolayer or bilayer-like arrangement (*10*). Many of the methylene chains are aligned approximately parallel to each other. It also appears as if there is a clear propensity for the orientation of the acyl chains to be perpendicular to the direction of the polypeptide strands of a β-sheet, somewhat between the side chain positions. This is also true for many of the linked methylene carbons shown in Figure 4A and lipids 9, 11, and 34 visible in Figure 4C. The probable reason is the formation of a more substantial lipid−protein interface, while maximizing van der Waals interactions with the nearby nonpolar residues.

Both the conformation and surroundings of lipids 3 and 4 are illustrated in Figure 4C. The representation occurs at the intersection of the C- and A-sheet domains between what at first appears to be two cavity openings. The domain interactions may be strengthened by the presence of the boundary lipid in this vicinity. Again, the largest cavity opening is shown at the bottom. The potential cavity opening shown at the top of the figure is buried by the presence of a second lipovitellin monomer. This covered opening is partly filled by lipid 3, which is modeled as phosphatidylethanolamine. Perhaps because the cavity wall formed by the peptide between the openings is shorter than a phospholipid bilayer, the hydrocarbon chains of lipids 3 and 4 appear to be essentially splayed, which allows occupancy of both sites with a bilayer-like arrangement.

The ethanolamine moiety of lipid 3 is involved in the only interaction found between the boundary lipid and the polypeptide from a symmetry-related subunit (N1038′, not depicted). Lipid 3 has the phosphate atom with the accompanying oxygen atoms interacting with bound solvent and the relatively close R592 (top, back). Here one may suspect that simple Coulombic interactions provide some stabilization energy. The phosphate part of lipid 4 also appears to have interactions to bound water molecules and electrostatic compensation from the close by K625 (shown) and R46. However, it is again evident from Figure 4C that the majority of interactions are nonpolar in nature.

Figure 4D contains an image of the electron density for one hydrocarbon chain, number 14. This is a very unusual position with all 16 carbon atoms of the methylene chain surrounded by protein atoms (see also Figure 5). No visible electron density is present for the headgroup to help to identify the lipid molecule. The protein atoms form a "cave" of a size just equal to the van der Waals radius of the methylene chain. Residues from the N- and A-sheets that define the site are given in Table 5. The significance of this unique location is obscure in terms of the overall formation of the main lipid domain far removed from this site.

The data shown in Figure 4E cover a portion of the smaller opening of the cavity centered on lipid 48. The appearance of the electron density suggests that three other hydrocarbon chains interact with this lipid. However, number 48 parallels the edge of the most exposed β-sheet, containing the interacting residues 1013−1016 (center of illustration). The

position and orientation of this feature are cause for some concern because the distance is nearly right for an extension to the β-sheet. The appearance of lipids 10, 22, 23, and 48 together may even argue for an extension by two β-strands and a β-turn of highly disordered polypeptide. Although perhaps due to the location at a cavity mouth, more bound water interacts with lipid 48 than is evident for the other purely hydrocarbon molecules. There is no information which indicates what protein residues might occupy this site. The visible ends of the closest segment of the missing peptide, residues 951−994, are about 25−35 Å away. Because it is equally possible that these features are not protein, the density was assigned to lipid 48.

A study of the interfacial interactions for all 50 lipid molecules, as derivable by ASA calculations (*37*), has been carried out, and the results are summarized in the histogram of Figure 5. These interface values are the sum of the ASA on both partners that become inaccessible to solvent. The buried surface areas for the 50 bound lipid segments are described for six types of interface. (1) The ASA of each lipid is given. Since most of this area lies within the binding cavity in which more lipids reside, these estimates are partly of the interface between the boundary lipid and that within the disordered core. (2) The ASA lost by shielding with bound solvent molecules was also calculated. The most significant data are the hydrophobic and remaining surface regions lost through interactions with neighboring lipid molecules (3 and 4), and for the buried area found between each lipid and the polypeptide atoms (5 and 6).

Variations in the total ASA for the different molecules are clearly related to variations in the length of the hydrocarbon chain visible in the electron density map: the more methylene carbons observed the more ASA. For every lipid atom that has been observed, most are unreachable by the 1.4 Å probe. Larger bound solvent interfaces are primarily found for the phospholipids, although the extent to which water molecules represent the headgroup atoms of numbers 2 and 4−7 is unknown. The lipid−protein inaccessible surface is the largest component for lipids 1, 3−5, 14, 21, 24−25, 30, 38, and 45. Not including the area in contact with disordered lipid, the buried area between lipid molecules is the greater constituent for lipids 6−7, 10, 12−13, 15−18, 20, 26−29, 34, 36, 40, 44, 46−48, and 50. Interestingly, for the lipid segment number's 20, 40, 42, 44, 47, and 50 essentially no interactions occur with lipovitellin. Hence these partial hydrocarbon chains must represent a second level of organization in the formation of the boundary lipid.

An important fraction of the lipid−lipid and lipid−protein interactions in Figure 5 can be described as nonpolar. The free energies involved in the loss of ASA accompanying binding are probably dominant. It has been proposed that there is a linear correlation between the change in the nonpolar buried surface and the change in the free energy of association in both experimental determinations of subunit−subunit interfaces (*38*) and theoretical analyses (*39*). An approximation of $\Delta(\Delta G^\circ) = -15$ to -16 cal/(mol·Å^2) for the free energy gain upon burial of 1 Å^2 of the hydrophobic surface has been used. The applicability of these approximations to the interaction of methylene carbons belonging to lipid molecules and proteins has not yet been studied.

Except for just a few instances involving very weak hydrogen bonds or charge stabilization, the preponderance of interactions appear quite nonspecific, mainly van der Waals interactions. Therefore, nearly all of the polar headgroups of the bound phospholipid are probably disordered. Presumably, the lack of specific hydrogen bonds may be an advantage for the developing organism. There are six major classes and hundreds of molecular species with different fatty acid substituents found in the mixture that is often referred to in the singular as phospholipid.

CONCLUSIONS

Crystalline lipovitellin contains about 16% w/w lipid, all of which is noncovalently bound. The low-temperature crystallographic studies increased the resolution considerably, and some electron density attributable to bound lipid was found at the reduced temperature. To avoid overinterpretation, a five-carbon limit was placed on any hydrocarbon chain. The results of refinement were the 50 segments of lipid included in the new X-ray coordinates.

Only seven of the identified segments contained visible electron density for the headgroups. The other 43 fragments resemble the expected acyl components of phospholipid, the often-called lipid "tails". The chiefly hydrophobic surface of the cavity accommodates this boundary lipid with little regard to their polar ends, suggesting that the specificity for phospholipid binding at the cavity wall is not great. Therefore, high-affinity binding of phospholipid headgroups may also not be a principal factor in the initial or nucleating lipid−protein interactions, except possibly for lipid 1, the sole phosphatidylcholine modeled.

Taken together, the positions of the 50 lipid molecules form a crude shell-like structure on the inner surface of what has been demonstrated by other studies to contain the associated lipid. For the most part where β-strands are present, the methylene chains of the associated lipid appear to run approximately perpendicular to the direction of the polypeptide chains. However, the acyl chains are also greatly twisted to accommodate the varying directions of the surrounding β-sheets. This boundary lipid should nucleate interactions with an anisotropic conformation of additional lipid propagating throughout the cavity core. In a few examples, lipid was found without any peptide interface. It would seem that, at a temperature of 100 K, noncovalent lipid−lipid interactions are sufficient to order some methylene segments. Finally, this lipovitellin structure provides additional support for the original model of a monolayer or bilayer organization for the bulk lipid.

ACKNOWLEDGMENT

We thank Ms. Judy Bratt for preparing crystals of lipovitellin and Dr. Joe Barycki for reviewing the manuscript. Most of the computing resources needed for the investigation came from the Minnesota Supercomputing Center, particularly from the Biomedical Sciences Computing Laboratory. Use of the Argonne National Laboratory Structural Biology Center beamlines at the Advanced Photon Source was supported by the Office of Biological and Environmental Research, U.S. Department of Energy, under Contract W-31-109-ENG-38. We also thank Drs. Norma E. C. Duke and Rongguang Zhang for help in collecting the diffraction data at the APS.

REFERENCES

1. Willnow, T. E. (1999) *J. Mol. Med. 77*, 306−315.
2. Byrne, B. M., Gruber, M., and Ab, G. (1989) *Prog. Biophys. Mol. Biol. 53*, 33−69.
3. Baker, M. E. (1988) *Biochem. J. 255*, 1057−1060.
4. Shoulders, C. C., Brett, D. J., Bayliss, J. D., Narcisi, T. M., Jarmuz, A., Grantham, T. T., Leoni, P. R., Bhattacharya, S., Pease, R. J., Cullen, P. M., Levi, S., Byfield, P. G. H., Purkiss, P., and Scott, J. (1993) *Hum. Mol. Genet. 2*, 2109−2116.
5. Shoulders, C. C., Narcisi, T. M., Read, J., Chester, A., Brett, D. J., Scott, J., Anderson, T. A., Levitt, D. G., and Banaszak, L. J. (1994) *Nat. Struct. Biol. 1*, 285−286.
6. Mann, C. J., Anderson, T. A., Read, J., Chester, S. A., Harrison, G. B., Kochl, S., Ritchie, P. J., Bradbury, P., Hussain, F. S., Amey, J., Vanloo, B., Rosseneu, M., Infante, R., Hancock, J. M., Levitt, D. G., Banaszak, L. J., Scott, J., and Shoulders, C. C. (1999) *J. Mol. Biol. 285*, 391−408.
7. Segrest, J. P., Jones, M. K., and Dashti, N. (1999) *J. Lipid Res. 40*, 1401−1416.
8. Raag, R., Appelt, K., Xuong, N. H., and Banaszak, L. (1988) *J. Mol. Biol. 200*, 553−569.
9. Sharrock, W. J., Rosenwasser, T. A., Gould, J., Knott, J., Hussey, D., Gordon, J. I., and Banaszak, L. (1992) *J. Mol. Biol. 226*, 903−907.
10. Anderson, T. A., Levitt, D. G., and Banaszak, L. J. (1998) *Structure 6*, 895−909.
11. Timmins, P. A., Poliks, B., and Banaszak, L. (1992) *Science 257*, 652−655.
12. Meininger, T., Raag, R., Roderick, S., and Banaszak, L. J. (1984) *J. Mol. Biol. 179*, 759−764.
13. Norberg, B., and Haux, C. (1985) *Comp. Biochem. Physiol. B81*, 869−876.
14. Banaszak, L. J., and Seelig, J. (1982) *Biochemistry 21*, 2436−2443.
15. Otwinowski, Z., and Minor, W. (1997) *Methods Enzymol. 276*, 307−326.
16. Read, R. (1999) *Acta Crystallogr. D 55*, 1759−1764.
17. Brünger, A. T., Adams, P. D., Clore, G. M., DeLano, W. L., Gros, P., Grosse-Kunstleve, R. W., Jiang, J. S., Kuszewski, J., Nilges, M., Pannu, N. S., Read, R. J., Rice, L. M., Simonson, T., and Warren, G. L. (1998) *Acta Crystallogr. D 54*, 905−921.
18. Jones, A. T., Zou, J. Y., Cowan, S. W., and Kjeldgaard, M. (1991) *Acta Crystallogr. A 47*, 110−119.
19. Levitt, D. G. (2001) *Acta Crystallogr. D 57*, 1013−1019.
20. Engh, R., and Huber, R. (1991) *Acta Crystallogr. A 47*, 392−400.
21. Hooft, R. W. W., Sander, C., Vriend, G., and Abola, E. E. (1996) *Nature 381*, 272.
22. Laskowskki, R. A., MacArthur, M. W., Moss, D. S., and Thorton, J. M. (1993) *J. Appl. Crystallogr. 26*, 283−291.
23. Lovell, S. C., Word, J. M., and Richardson, J. S. (2000) *Proteins 40*, 389−408.
24. Perrakis, A., Sixma, T. A., Wilson, K. S., and Lamzin, V. S. (1997) *Acta Crystallogr. D 53*, 448−455.
25. van den Akker, F., and Hol, W. G. J. (1999) *Acta Crystallogr. D 55*, 206−218.
26. MacArthur, M. W., and Thorton, J. M. (1996) *Protein Eng. 8*, 217−224.
27. Network, E.-D. V. (1998) *J. Mol. Biol. 276*, 417−436.
28. Vlassi, M. D. Z., Wilson, K. S., and Kokkinidis, M. (1998) *Acta Crystallogr. D 54*, 1245−1260.
29. Addlagatta, A., Krzywda, S., Czapinska, H., Otlewski, J., and Jaskolski, M. (2001) *Acta Crystallogr. D 57*, 649−663.
30. Allen, F. H., and Kennard, O. (1993) *Chem. Des. Autom. News*, 31−7.
31. Schlenkrich, M., Brickmann, J., MacKerell, A. D., Jr., and Karplus, M. (1996) *Biological Membranes: A Molecular Perspective from Computation and Experiment* (Merz, K. M., and Roux B., Eds.) pp 31−81, Birkhauser, Boston.
32. Kleywegt, G. J., and Brünger, A. T. (1996) *Structure 4*, 897−904.
33. Lovell, S. C., Word, J. M., Richardson, J. S., and Richardson, D. C. (2000) *Proteins 40*, 389−408 (see also http://kinemage.biochem.duke.edu/validation/model.html#rama).
34. Luzzati, V. (1952) *Acta Crystallogr. A 5*, 808−810.
35. Read, R. J. (1986) *Acta Crystallogr. A 42*, 140−149.
36. Liang, J., Edelsbrunner, H., and Woodward, C. (1998) *Protein Sci. 7*, 1884−1897.
37. Lee, B., and Richards, F. (1971) *J. Mol. Biol. 55*, 379−400.
38. Vallone, B., Miele, A. E., Vecchini, P., Chiancone, E., and Brunori, M. (1998) *Proc. Natl. Acad. Sci. U.S.A. 95*, 6103−6107.
39. Eisenberg, D., and McLachlan, A. D. (1986) *Nature 319*, 199−203.

BI025674W